

# White organic light-emitting diodes based on C545T doped emitting system

Hua-Ping Lin<sup>\*1</sup>, Fan Zhou<sup>1</sup>, Jun Li<sup>1,2</sup>, Xiao-Wen Zhang<sup>3</sup>, Liang Zhang<sup>1</sup>, Xue-Yin Jiang<sup>1,2</sup>, Zhi-Lin Zhang<sup>1,2</sup>, and Jian-Hua Zhang<sup>1,2</sup>

<sup>1</sup>Department of Materials Science, Shanghai University, Jiading, Shanghai 201800, People's Republic of China

<sup>2</sup>Key Laboratory of Advanced Display and System Applications, Ministry of Education, Shanghai University, Shanghai 200072, People's Republic of China

<sup>3</sup>Guangxi Key Laboratory of Information Materials, Guilin University of Electronic Technology, Guilin 541004, People's Republic of China

Received 31 August 2011, revised 14 October 2011, accepted 11 November 2011

Published online 1 December 2011

**Keywords** C545T, energy transfer, Forster's radius, WOLEDs

\* Corresponding author: e-mail huapinglin@yahoo.com, Phone: +86-15201931788, Fax: +86-21-39988216

Fluorescent white organic light-emitting diodes (WOLEDs) with single-emitting layer (EML) and double-EML structures were demonstrated using a 2,3,6,7-tetrahydro-1,1,7,7-tetramethyl-1H,5H,11H-10(2-benzothiazolyl)quinolizine-[9,9a,1gh]-coumarin (C545T) doped emitting system. With the incorporation of double-EML structure, white emission with Commission Internationale de L'Eclairage (CIE) color coordinates of

(0.331, 0.335) and luminous efficiency of 8.04 cd/A was obtained. Moreover, WOLED with a single-EML structure shows superior electroluminescence performances such as lower voltage, higher luminance, and enhanced power efficiency. These improvements are attributed to its high energy transfer ability via the intermediation of C545T. The Forster's radius was given to clarify the actual energy transfer process.

© 2011 WILEY-VCH Verlag GmbH & Co. KGaA, Weinheim

**1 Introduction** White organic light-emitting diodes (WOLEDs) have attracted much interest due to their potential applications in flat-panel displays and solid-state lighting sources since the pioneer work of Tang and VanSlyke [1–3]. Commercial applications of OLED require high brightness, efficiency, and extended lifetime. To meet these requirements, light emission at a low driving voltage is necessary, since high driving voltage will reduce device lifetime because of thermal aging and impurity diffusion problems [4, 5]. Common approaches for obtaining white light include color mixing from a multilayer structure in which each emissive layer (EML) emits red, green, and blue colors [6], using a single layer structure which consists of different dyes doped into the same host [7], using exciplex formation [8], and using the microcavity effect [9]. In particular, most of the researches used the single-EML or multiple-EML structure to fabricate WOLEDs. For single-EML structure, it offers easy fabrication and better color stability, while its electroluminescent (EL) efficiency is usually low [10, 11]. Multiple-EML WOLEDs shows much higher efficiency than that of single-EML devices, but its Commission Internationale de L'Eclairage (CIE)  $x$ ,  $y$

coordinates are often dependent upon driving voltage, which is due to the shift of the exciton-recombination zone [12–14]. In recent years, steady progress has been made in improving the performances using various structures and materials [4–14]. However, the fabrication of high performance devices is still difficult. The precise control of dopants, the demand for an appropriate stacking sequence and thickness of EMLs are all important factors to improve the efficiency and color stability. Therefore, it is a great challenge to develop WOLEDs with sufficient efficiency, stable color coordinates, and low driving voltage.

We constructed two kinds of Blue OLEDs (BOLEDs) based on double-dopant and double-EML structures [15]: (1) the 2,3,6,7-tetrahydro-1,1,7,7-tetramethyl-1H,5H,11H-10(2-benzothiazolyl)quinolizine-[9,9a,1gh]coumarin (C545T) based BOLED with single-EML structure showed an efficiency of 4.64 cd/A and CIE coordinates of (0.166, 0.242). (2) The C545T based BOLED with double-EML structure showed an efficiency of 6.31 cd/A and CIE coordinates of (0.155, 0.212). The double-EML BOLED shows a striking improvement in color chromaticity and luminous efficiency as compared to the corresponding

single-EML counterpart. These excellent performances partly result from effective energy transfer in the emitting system. For color display applications, blue emitter is indispensable component for generating white emission and its performance is critical to that of white emitter. In order to fabricate high performance WOLEDs, in this paper, we select the same structure as mentioned above owing to its facile fabrication and efficient energy transfer. Two issues have been solved. First, direct energy transfer from 4, 40-bis (2, 2-diphenylvinyl)-1, 10-biphenyl (DPVBi) to 4-(dicyanomethylene)-2-t-butyl-6(1,1,7,7-tetramethyljulolidyl-9-enyl)-4H-pyran (DCJTB) is not efficient due to its wide band gap and reduced overlap emission of DPVBi and absorption of DCJTB. As the intermediation of C545T, an efficient white emission can be achieved through the cascade energy transfer from DPVBi to C545T and then from C545T to DCJTB. Second, a widely used approach for evaluating energy transfer in a doped emitting system is to calculate Förster's radius. The Förster's radius is proposed to understand the actual process of energy transfer in C545T-doped emitting system.

**2 Experimental** The WOLEDs were fabricated on indium tin oxide (ITO) coated glass substrate with a sheet resistance of  $20 \Omega/\square$ . After routine cleaning, the ITO was further treated by UV ozone for 10 min. The organic layers and cathode were thermally deposited at  $1.0 \times 10^{-6}$  Torr. The organic layers and the cathode LiF/Al were sequentially deposited by conventional vacuum vapor deposition in the same chamber without breaking the vacuum. The thickness of the deposited materials was controlled by using a quartz-crystal monitor. The composite film was prepared from simultaneous co-deposition of host and dopants. The configuration in this study is as described as follows and shown in Fig. 1.

**Cell-S:** ITO/MoO<sub>x</sub> (4 nm)/NPB (30 nm)/DPVBi: 5% 1, 4-bis [2-(3-N-ethylcarbazoyl) vinyl] benzene (BCzVB): 0.075% C545T: 0.125% DCJTB (20 nm)/BPhen (15 nm)/LiF/Al.

**Cell-D:** ITO/MoO<sub>x</sub> (4 nm)/NPB (30 nm)/DPVBi: 5% BCzVB (2 nm)/DPVBi: 5% BCzVB: 0.075% C545T: 0.125% DCJTB (20 nm)/BPhen (15 nm)/LiF/Al.

The MoO<sub>x</sub> was used as the hole injection layer, N,N'-di (naphthalene-1-y1)-N,N'-dipheyl-benzidine (NPB) was used as the hole transport layer, 4-7-diphenyl-1, 10-phenanthroline (BPhen) was used as the electron transport layer, LiF was used as the electron injection layer [16], respectively. The EML with single (Cell-S) and double (Cell-D) structures was sandwiched between hole transport layer and electron transport layer. DPVBi doped with BCzVB was used as the blue matrix [7]. Here, BCzVB functioned as an assistant dopant to improve the efficiency of blue matrix. C545T was used as the green dopant [15], DCJTB was used as the red dopant [7], respectively.

The active area of the devices was  $5 \times 5 \text{ mm}^2$ . The EL spectra and Commission Internationale d'Eclairage (CIE) color coordinates were measured by a PR-650 Spectra Scan.

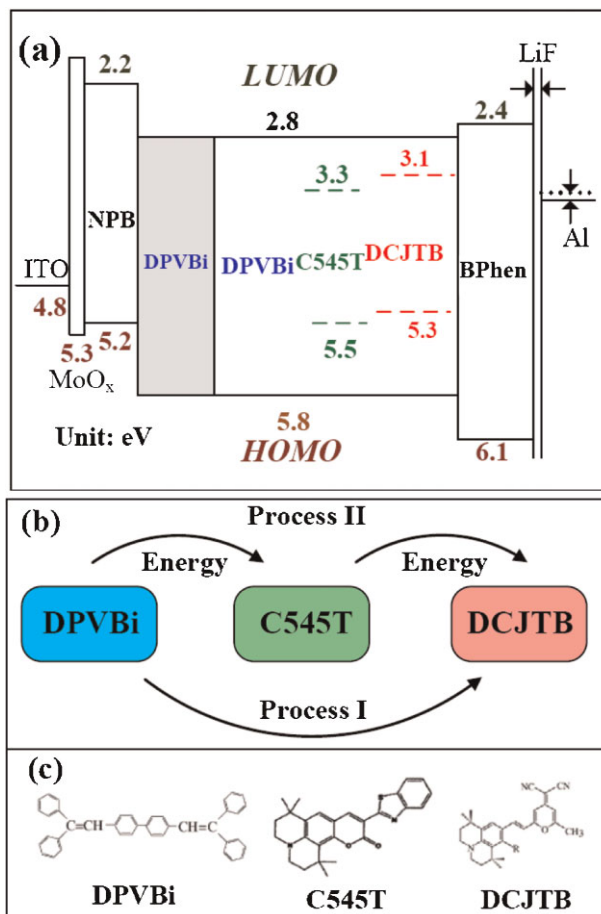


**Figure 1** (online color at: [www.pss-a.com](http://www.pss-a.com)) The configuration of devices (a), process of energy transfer (b), and molecular structures of organic materials (c).

The current–voltage–luminance (*I–V–L*) measurements were performed using a Keithley 2400 Source Meter and a Minolta LS-110 luminance meter. The photoluminescent (PL) spectra and optical absorption (Abs) spectra were taken with a Hitachi 850 fluorescence spectrophotometer.

**3 Results and discussion** The normalized EL spectra at a current density of  $20 \text{ mA/cm}^2$  are illustrated in Fig. 2. It is noted that blue emission from the blue matrix of DPVBi (at 456 nm) matches green emission from C545T (at 492 nm) and red emission from DCJTB (at 572 nm), resulting in white emission. Although the concentration of DCJTB is very low, emission from DCJTB can be strong. This is due to C545T assistance effect which is beneficial to energy transfer (which will be discussed later); otherwise the energy transfer from DPVBi to DCJTB is poor. It can be seen that color purity is considerably improved when the double-ETL structure is used. For example, at the current density of  $20 \text{ mA/cm}^2$ , emissive color shifts from reddish white (Cell-S) to pure white (Cell-D) with the corresponding CIE color coordinates changing from (0.342, 0.346) to (0.331, 0.335). In addition, both devices show excellent color stability, i.e.,

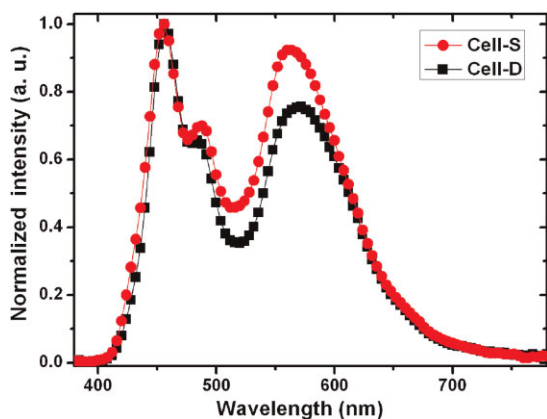


**Figure 2** (online color at: www.pss-a.com) Normalized EL spectra of these devices at the current density of 20 mA/cm<sup>2</sup>.

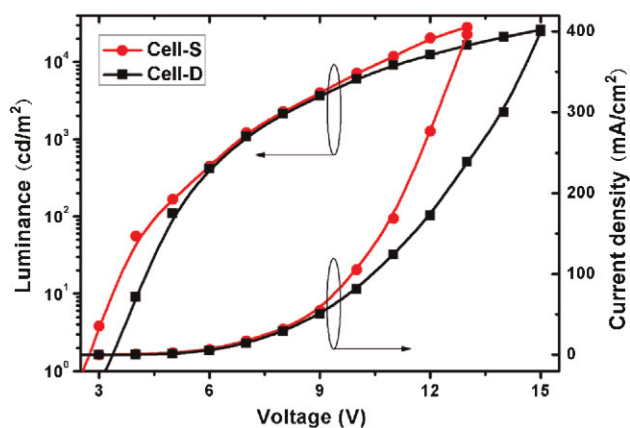


**Figure 3** (online color at: www.pss-a.com) Current–voltage and luminance–voltage characteristics of the devices.

slight EL color shift with varying drive currents. For instance, the CIE  $x$ ,  $y$  color coordinates shift only from (0.343, 0.347) at 4 mA/cm<sup>2</sup> to (0.339, 0.345) at 200 mA/cm<sup>2</sup> with  $\Delta_{x,y} = \pm[0.004, 0.002]$  for Cell-S. At the same time, the CIE coordinates shift from (0.331, 0.337) to (0.328, 0.334) with  $\Delta_{x,y} = \pm[0.003, 0.003]$  for Cell-D within the same current variation.

Figure 3 shows the current density–voltage and luminance–voltage characteristics for Cell-S and Cell-D. The main performances of the two devices are listed in Table 1. It can be seen that Cell-S shows lower voltage, but higher

current density and emission intensity. For instance, at the current density of 20 mA/cm<sup>2</sup>, the driving voltage for Cell-S is 7.1 V, while Cell-D has higher voltages of 7.8 V. Similarly, the turn-on voltage (defined as the voltage to achieve the luminance of 1 cd/m<sup>2</sup>) of Cell-S is 2.8 V, which is 0.3 V lower than that of Cell-D. In Cell-D, excitons can be generated in the interface between the NPB/first EML interface [17]. The generated excitons diffuse into the first EML and then cause luminescence on recombination in this layer. The remaining excitons enter into the second EML and, in the same way, produce luminescence of this layer. According to the energy level diagram in Fig. 1, DPVBi possesses a deep highest occupied molecular orbital (HOMO) level of 5.8 eV. It is expected to behave as an effective blocking site for holes. With the incorporation of double-EML structure in Cell-D, the first EML of DPVBi can greatly impede holes to enter the second EML. The blocked hole injection results in a smaller amount of holes available travel into the second EML and recombine with electrons. This huge barrier for energy transfer could increase the driving voltage. In Cell-S, excitons are generated at the NPB/single-EML interface. The energy levels of C545T are located between that of DPVBi and DCJTb. The cascade energy transfer from DPVBi to DCJTb via the intermediation of C545T can occur in this device. This indicates energy transfer is responsible for the changes in carrier mobility, and thereby reduces the driving voltage. On the other hand, the increase in voltage in Cell-D may be in relation to an increase of thin-film resistance, which is ascribed to the increase of the thin-film thickness. For these two cases, the former would be dominant because the increase in thickness is only 2 nm. In addition, efficient energy transfer from matrix to guest plays a significant role in promoting emission intensity [18]. It is interesting to note that Cell-S achieves a maximum luminance of 28 160 cd/m<sup>2</sup> at 13 V. This could be in relation to the high energy transfer ability of Cell-S as compared to Cell-D.

The power and luminous efficiencies are shown in Fig. 4. It can be seen that Cell-S shows a maximum power efficiency of 5.62 Lm/W, while Cell-D has a lower efficiency of 5.05 Lm/W. The reduction in driving voltage corresponds to enhancement of power efficiency. It is well known that injection current is very sensitive to the barrier height, and the device efficiency is mainly determined by the number of minority carriers (electrons in this study). On the other hand, Cell-S shows a bit lower luminous efficiency because of excess hole injection and thus an unbalance of electrons and holes, a weak current-induced fluorescence quenching is also

**Table 1** Characteristics of these devices at 20 mA/cm<sup>2</sup>; the values inside the brackets were the maximum.

	luminance (cd/m <sup>2</sup> )	voltage (V)	$\eta_L$ (cd/A)	$\eta_p$ (Lm/W)	CIE ( $x$ , $y$ )	CIE <sup>c</sup> ( $x$ , $y$ )
Cell-S	1.465 (28.160, 13 <sup>a</sup> )	7.1 (2.8 <sup>b</sup> )	7.11 (7.30)	3.15 (5.62)	(0.342, 0.346)	(0.004, 0.002)
Cell-D	1.821 (26.124, 15 <sup>a</sup> )	7.8 (3.1 <sup>b</sup> )	7.46 (8.04)	2.92 (5.05)	(0.331, 0.335)	(0.003, 0.003)

<sup>a</sup>The driving voltage corresponding to the maximum brightness. <sup>b</sup>The turn-on voltage defines as the voltage to achieve the luminance of 1 cd/m<sup>2</sup>. <sup>c</sup>The CIE color coordinate migration from 4 to 200 mA/cm<sup>2</sup>.

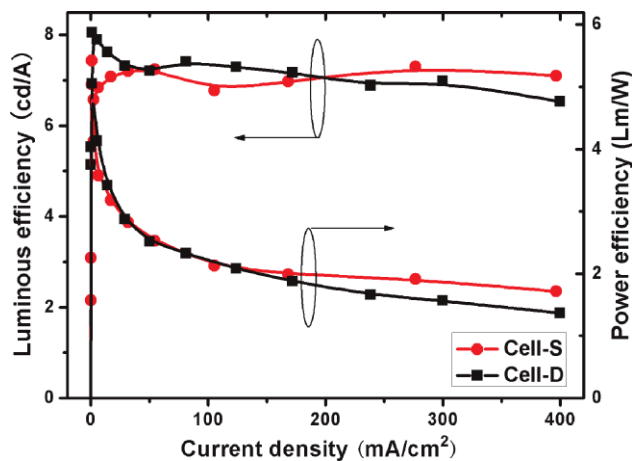


**Figure 4** (online color at: [www.pss-a.com](http://www.pss-a.com)) The power and luminous efficiencies-current density curves of the devices.

observed. In our device, the enhancement of energy transfer reduces the accumulation of holes at the interfaces and lowers local aggregation of the molecules at the interface [19], which greatly contributes to the improvement in stability of the device and thus, the current-induced fluorescence quenching has been mostly controlled. From Fig. 4, one can see that Cell-S shows no obvious efficiency drop. It follows that the luminous efficiency of Cell-S exceeds that of Cell-D at the high current density of 200–400 mA/cm<sup>2</sup>.

In common, the excitation mechanism in doped OLEDs is considered to be energy transfer, carrier trapping, or both [20]. The enhancement of efficiency could readily be realized with judicious selection of matching dopants for more electron and hole recombination. It can be seen in Fig. 1b that there are two possible processes in Cell-S, Process I: injected electrons and holes recombine on the host material of DPVBi. The DPVBi enter an excited state and then the excitonic energy is transferred to the DCJTB sites by the energy transfer process and the DCJTB molecules produce white emission.

Process II: Injected electrons and holes recombine on the host material of DPVBi. The DPVBi enter an excited state and then the excitonic energy is transferred from DPVBi to C545T and then from C545T to the DCJTB sites by the energy transfer process to produce the white emission.

As mentioned previously, the energy levels of C545T located between that of DPVBi and DCJTB. Therefore, injected holes and electrons can be efficiently transferred from DPVBi to the corresponding HOMO and LUMO (lowest unoccupied molecular orbital) levels of C545T. Then, excitation energy of C545T can be transferred efficiently to DCJTB. To further understand energy transfer property, the probability of energy transfer can be evaluated by calculating of Förster's radius ( $R_0$ ). In the Förster's mechanism, the dipole-dipole interaction results in efficient energy transfer of the singlet excited-state energy from the

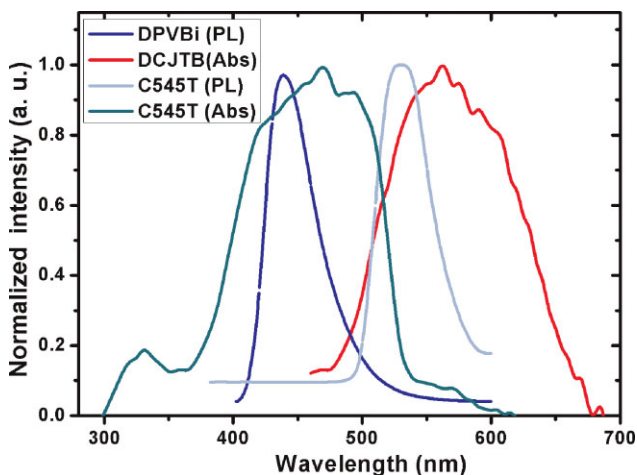


**Figure 5** (online color at: [www.pss-a.com](http://www.pss-a.com)) PL emission and absorption spectra of DPVBi, C545T, and DCJTB measured in dichloromethane solution.

host to the dopants, which reflects the necessity of energetic resonance during the transition. It is expressed by [21]:

$$R_0^6 = \frac{0.5291\beta^2}{N_A n^4} \int_0^\infty F_M(\nu) \varepsilon_A(\nu) \frac{d\nu}{\nu^4}, \quad (1)$$

where  $\nu$  is the wavenumber,  $\varepsilon_A(\nu)$  is the molar decadic extinction coefficient,  $\beta^2$  is an orientation factor (2/3 for random orientation),  $N_A$  is the Avogadro's number, and  $n$  is the refractive index of the host material. To understand the process of energy transfer, we measured the PL emission spectra of the host (DPVBi) and Abs spectra of dopants (C545T and DCJTB), as shown in Fig. 5. The calculated Förster's radius from DPVBi to DCJTB is 12.9 Å. Furthermore, Förster's radius from DPVBi to C545T is 51.6 Å and from C545T to DCJTB is 55.4 Å, respectively. It suggests that the energy transfer from DPVBi to DCJTB via the intermediation of C545T (Process II) seems to be more dominant than that from DPVBi directly to DCJTB (Process I). It can also be seen from a little overlap between the PL spectra of DPVBi and Abs spectra of DCJTB that the direct energy transfer is not efficient because the energy transfer is proportional to the overlap area.

**4 Conclusion** This paper presents two kinds of C545T based WOLEDs, which is fabricated using single-EML and double-EML structures. With the incorporation of double-EML structure, white emission with CIE color coordinates of (0.331, 0.335) and luminous efficiency of 8.04 cd/A was obtained. Furthermore, WOLED with a single-EML structure shows superior electroluminescence performances such as lower voltage, higher luminance, and enhanced power efficiency. The significant improvements in device performance are attributed to high energy transfer ability via the intermediation of C545T. The Förster's radius is proposed to understand the actual process of energy transfer.

**Acknowledgements** The authors would like to acknowledge the financial supports of the National Natural Science Foundation of China (60777018, 60776040, and 61077013), 863 projects (2008AA03A336 and 2010AA3A337), Shanghai Science and Technology Committee (06DZ22013), Shanghai Leading Academic Disciplines (S30107), the Project of National Post-Doctor Fund (2011M500569) and Shanghai University Graduates' Innovation Fund (SHUCX111019 and SHUCX112223).

## References

- [1] C. W. Tang and S. A. VanSlyke, *Appl. Phys. Lett.* **51**, 913 (1987).
- [2] Y. F. Li, F. Li, J. H. Zhang, C. L. Wang, S. J. Zhu, H. J. Yu, Z. H. Wang, and B. Yang, *Appl. Phys. Lett.* **96**, 153305 (2010).
- [3] S. Reineke, F. Lindner, G. Schwartz, N. Seidler, K. Walzer, B. Lüssem, and K. Leo, *Nature* **459**, 234 (2009).
- [4] S. Gardonio, L. Gregoratti, P. Melpignano, L. Aballe, V. Biondo, R. Zamboni, M. Murgia, S. Caria, and M. Kiskinova, *Org. Electron.* **8**, 37 (2007).
- [5] I. D. Parker, Y. Cao, and C. Y. Yang, *J. Appl. Phys.* **85**, 2441 (1999).
- [6] R. L. Song, Y. Duan, S. F. Chen, Y. Zhao, J. Y. Hou, and S. Y. Liu, *Semicond. Sci. Technol.* **22**, 728 (2007).
- [7] H. P. Lin, D. B. Yu, X. W. Zhang, J. Li, L. Zhang, X. Y. Jiang, and Z. L. Zhang, *Semicond. Sci. Technol.* **25**, 105004 (2010).
- [8] J. Feng, F. Li, W. B. Gao, S. Y. Liu, Y. Liu, and Y. Wang, *Appl. Phys. Lett.* **78**, 3947 (2001).
- [9] W. Y. Ji, L. T. Zhang, T. Y. Zhang, W. F. Xie, and H. Z. Zhang, *Org. Electron.* **11**, 202 (2010).
- [10] C. H. Chuen and Y. T. Tao, *Appl. Phys. Lett.* **81**, 4499 (2002).
- [11] J. Kido and H. Shionoya, *Appl. Phys. Lett.* **67**, 2281 (1995).
- [12] G. H. Zhang, H. H. Chou, X. Q. Jiang, P. P. Sun, and C. H. Cheng, *Org. Electron.* **11**, 1165 (2010).
- [13] K. O. Cheon and J. Shinara, *Appl. Phys. Lett.* **81**, 1738 (2002).
- [14] K. O. Cheon and J. Shinara, *Appl. Phys. Lett.* **83**, 2073 (2003).
- [15] H. P. Lin, X. W. Zhang, D. B. Yu, J. Li, L. Zhang, F. Zhou, X. Y. Jiang, and Z. L. Zhang, *J. Optoelectron. Adv. Mater.* **12**, 2355 (2010).
- [16] H. P. Lin, F. Zhou, X. W. Zhang, D. B. Yu, J. Li, L. Zhang, X. Y. Jiang, and Z. L. Zhang, *Synth. Met.* **161**, 1133 (2011).
- [17] M. A. Khan, W. Xu, J. Cao, Y. Bai, W. Q. Zhu, X. Y. Jiang, and Z. L. Zhang, *Displays* **28**, 26 (2008).
- [18] L. Z. Yu, X. Y. Jiang, Z. L. Zhang, L. R. Lou, and C. T. Lee, *J. Appl. Phys.* **105**, 013105 (2009).
- [19] C. Adachi, K. Nagai, and N. Tamoto, *Appl. Phys. Lett.* **66**, 2679 (1995).
- [20] Y. Z. Wu, X. Y. Zheng, W. Q. Zhu, R. G. Sun, X. Y. Jiang, Z. L. Zhang, and S. H. Xu, *Appl. Phys. Lett.* **83**, 5077, (2003).
- [21] T. Förster, *Discuss. Faraday Soc.* **27**, 7 (1959).